Electronic Supplementary Information

A new polymorph of strontium hexaferrite stabilized at the nanoscale

D. Makovec,* G. Dražić, S. Gyergyek, D. Lisjak

Materials

Iron (III) nitrate heptahydrate ($Fe(NO_3)_3 \cdot 7H_2O$, strontium nitrate ($Sr(NO_3)_2$), sodium hydroxide (NaOH), nitric acid (HNO_3) were purchased from Alfa Aesar. Accurate concentrations of the metal ions in the nitrates were determined using optical emission spectroscopy with inductively coupled plasma (Agilent 720).

Characterization

For the transmission (TEM) and scanning-transmission (STEM) electron microscopy studies, the nanoplatelets were suspended in ethanol and deposited on a copper-grid-supported lacy carbon foil.

The TEM analyses were performed using a field-emission electron-source TEM Jeol 2010F operated at 200 kV. The nanoplatelet widths were estimated from TEM images by visual measurements using DigitalMicrograph™ Gatan Inc. software. The longest dimension of each measured NPL was considered as the NPL width. The thickness for the NPLs was measured oriented with the c-axis of their hexagonal structure perpendicular to the electron beam.

For the STEM analyses a probe Cs-corrected Jeol ARM 200CF STEM was operated at 80 kV. During the analysis of the samples, HAADF and ABF detectors were used simultaneously at 68–180 and 10–16 mrad collection semi-angles, respectively. To minimize the specimen drift, images were taken several hours after the insertion of the sample into the microscope and at least 20 minutes after the last sample positioning to minimize the goniometer drift. The chemical composition was analyzed using a Jeol Centurio EDXS system with a 100-mm^2 SDD detector.

The room-temperature magnetization $\boldsymbol{M}$ as a function of the magnetic field $\boldsymbol{H}$ of the samples was measured using a Lake Shore 7307 vibrating-sample magnetometer (VSM) with a maximum applied field of 10 kOe.

Thermal analyses were performed with a thermogravimetry and simultaneous differential scanning calorimeter (TGA/DSC 2, Mettler Toledo). The sample was heated from 40 °C to 700 °C at 10 °C/min in a static atmosphere of air.

Raman spectra of the powdered samples were recorded at room temperature using NT-MDT model Integra Spectra for Materials Science equipped with a confocal microscope. The 633-nm line of a helium-neon laser was used for the excitation. Scattered light was detected by a cooled CCD camera and a 600-grooves/mm grating. Spectral resolution of the system is 5 cm^{-1}. To obtain a good signal-to-noise ratio, 10 spectra of each sample measured for 60 s were collected. Before and after acquisition, the spectra were recorded at the same position and checked for possible damage induced by the laser irradiation. Spectra showed the same characteristics, indicating that no beam damage occurred during acquisition.

Thermal analysis

A TGA curve of the SF110 sample shows continuous mass loss up to approximately 450 °C. A large part of the total loss (~6%) occurred at temperatures below 150 °C and can be attributed to the desorption of physisorbed water. At higher temperatures the loss can be ascribed to the decomposition of carbonates. The total mass loss of 12.5 % is consistent with the high surface area of the NPLs and is similar to that observed for as-synthesized Ba-ferrite NPLs.[S1] In any case, the processes resulting in a mass loss were completed below 500 °C. Even if FeOOH were to be present in the SF110 sample, it would decompose during annealing at 500 °C and would not be present in the SF500 sample. Moreover, the structural rearrangement during the transformation of ferrihydrite to well-ordered hematite is marked by an exothermic effect at approximately 400 °C,[S2] not visible in the DTA curve of the SF110 NPLs.

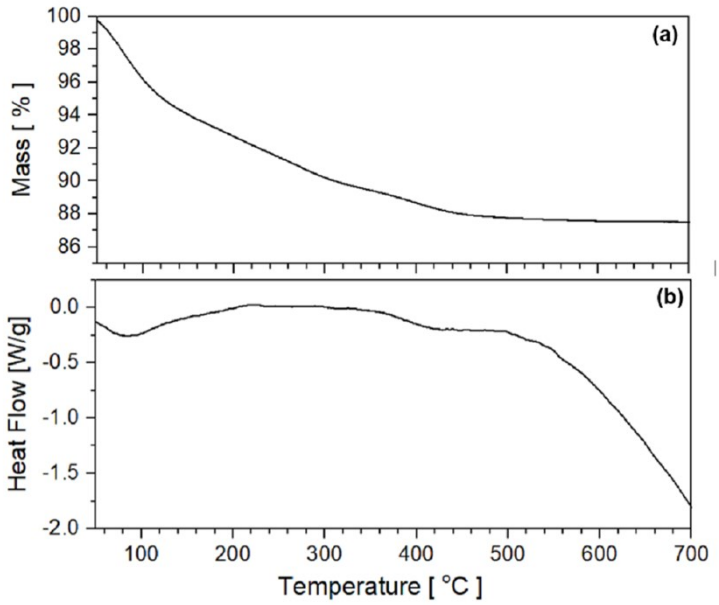

Fig. SI1. Thermal analysis of SF110 NPLs: TGA (a) and DSC (b).

Raman spectroscopy

Barium hexaferrite has a rich spectrum with 42 Raman active modes.[S3] The most intense are centered at 614 cm^{-1}, 684 cm^{-1} and 713 cm^{-1}, assigned to the vibrations of Fe octahedra in the R block, Fe bipyramids in the R block and Fe tetrahedra in the S block, respectively.[S3] The Raman spectrum of the SF110 (Fig. SI2) shows only a broad maximum in the range between 600 cm^{-1} and 750 cm^{-1}, indicating structural disorder and a small crystallite size. Because of its breadth it is difficult to assign it to a specific compound. It could be interpreted as structurally disordered hexaferrite or ferrihydrite, the only compound among various Fe oxides and oxyhydroxides that exhibits a single strong band centered at 712 cm^{-1}.[S2,S4] The Raman spectrum of SF160 (Fig. SI2) shows similar features as the spectrum of SF110, with one important difference, a clear appearance of a narrow band characteristic for Fe bipyramids in the R block of the hexaferrite structure. Ferrihydrite is thermally unstable and transforms to hematite (directly or forming maghemite as the intermediate phase) under laser irradiation of powers typical for Raman spectroscopy.[S5] In neither spectrum did we observe bands characteristic of hematite or maghemite (Fig. 2). It is then reasonable to conclude that samples SF110 and SF160 contain hexaferrite-like structures with significant disorder, while in the sample SF160 bipyramidal sites appear more ordered. Interestingly, the Raman spectrum of the annealed sample SF500 exhibits one broad maximum, indicating a poorly ordered structure. In contrast, sample SF700 shows Raman features characteristic for the bulk barium hexaferrite structure.[S5]

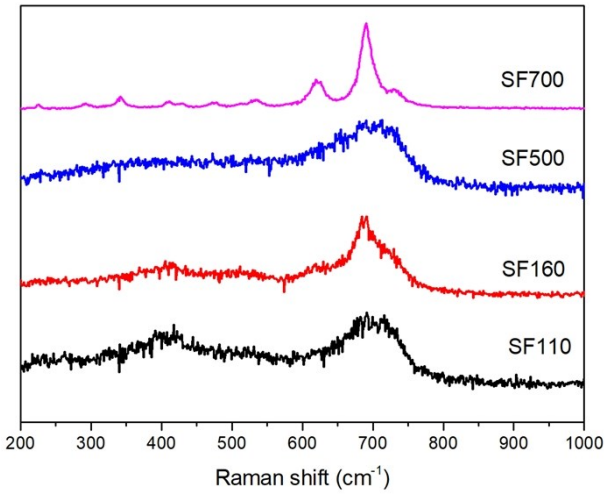

Fig. SI2. Raman spectra of different Sr-ferrite NPLs.

HAADF-STEM images of exaggeratedly grown nanoplatelets

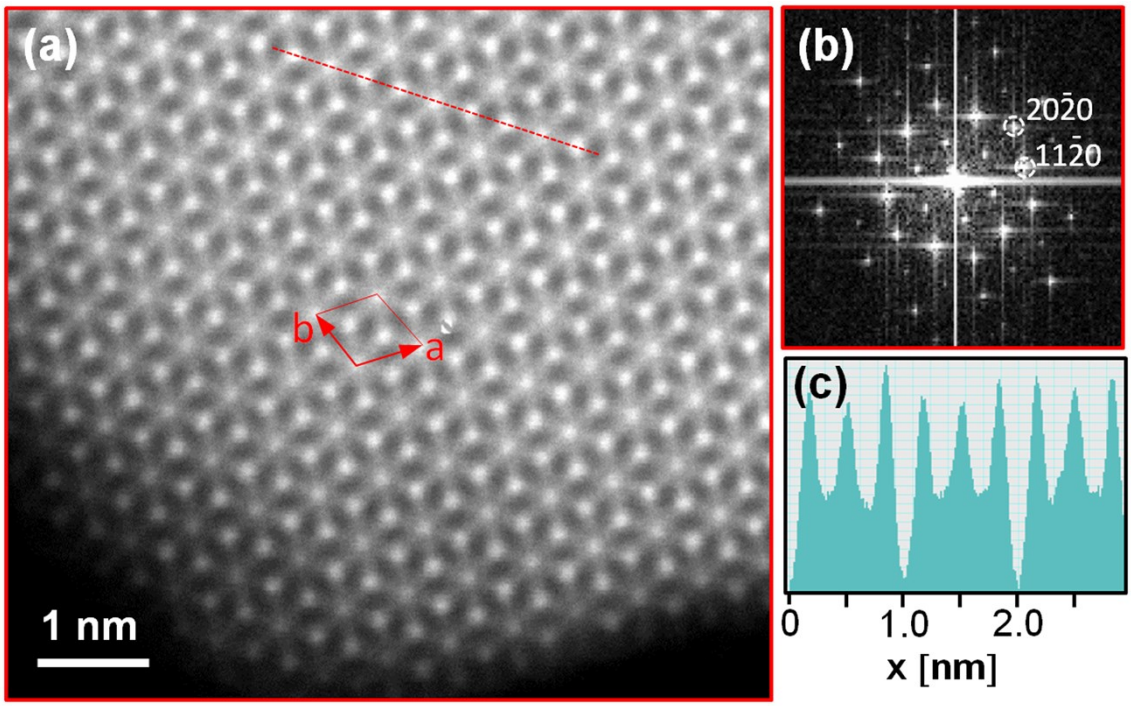

Fig. SI3. HAADF image (a) of NPL from SF200 sample and calculated FTT pattern (b) indexed according to the magnetoplumbite structure along the [0001] direction. (c) Intensity profile along the [10-10] direction (along dashed line in HAADF image).

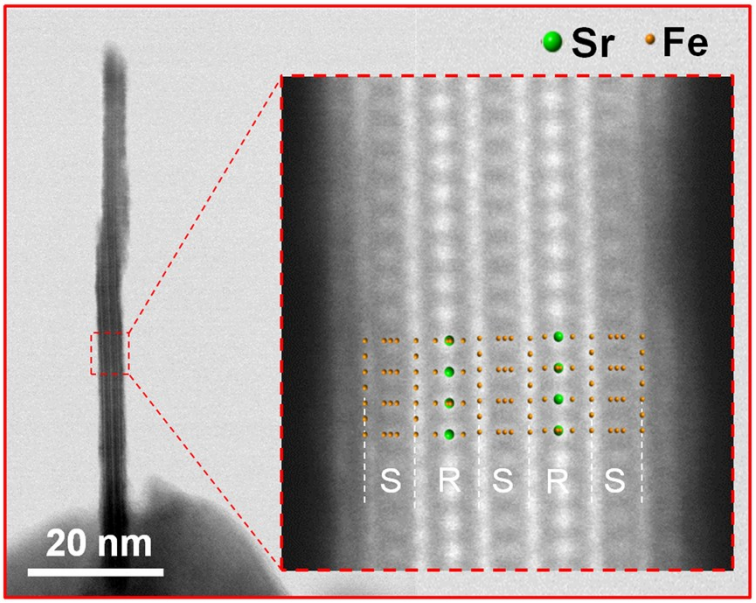

Fig. SI4. BF and HAADF STEM images of very thin, exaggeratedly grown NPL from SF200 sample. The projected model of the magnetoplumbite structure (in [11-20] zone axis) is superimposed over the image to illustrate the positions of the Sr^{2+} and Fe^{3+} columns. The NPL exhibits the SRS*R*S structure.

HAADF-STEM images of discoid nanoplatelets

In the magnetoplumbite Sr ferrite, we can see a clear difference between the $2Fe^{3+}$ columns (marked with smaller brown spots in Fig. 4 (a)) and the $4Fe^{3+}$ columns (larger brown spots), which are only slightly less bright than the $Sr^{2+}+4Fe^{3+}$ columns (green spots)). In the projection of the a-b plane, the $4Fe^{3+}$ column is surrounded by the six $2Fe^{3+}$ columns. The relative intensity of these columns surrounded by six neighboring columns on the HAADF image of discoid NPLs (Fig. 5(b)) is much weaker compared to that of the magnetoplumbite (Fig. SI5 (c)).

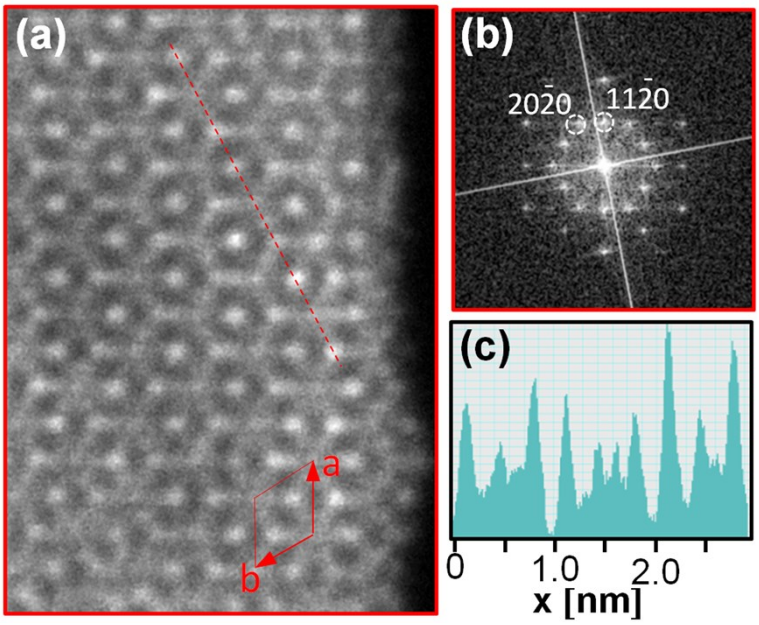

Fig. SI5. BF (a) and HAADF (b) images of the discoid NPL from the SF160 sample. Inset of (a) is the calculated FFT of the upper part of the NPL. (a) indexed as a hexagonal phase in the [0001] zone axis. (d) Intensity profile along the [10-10] direction (along dashed line in HAADF image (b)).

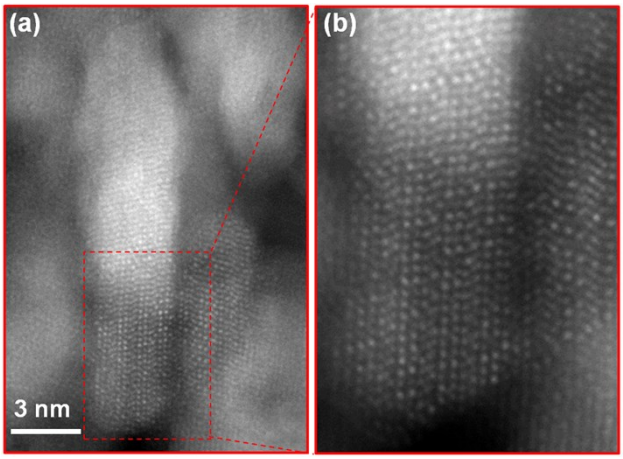

Fig. SI6. HAADF STEM images of small, discoid NPLs from the SF110 sample.

HAADF-STEM images of annealed nanoplatelets

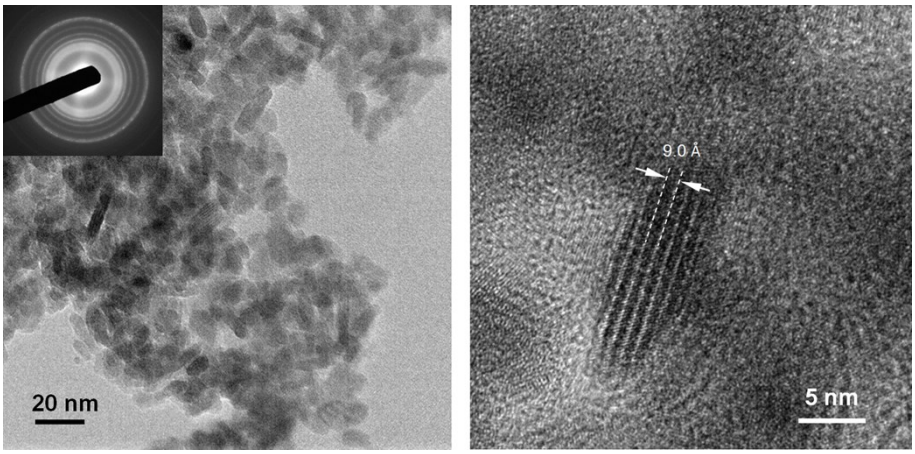

Fig. SI7. (a) TEM image with corresponding electron diffraction pattern SF110 NPLs after annealing for 2 hours at 500 °C. (b) HREM lattice image of the NPL oriented edge-on. The periodicity of the lattice fringes across the NPL of 0.9 nm corresponds to the (002) planes of the new polymorph structure.

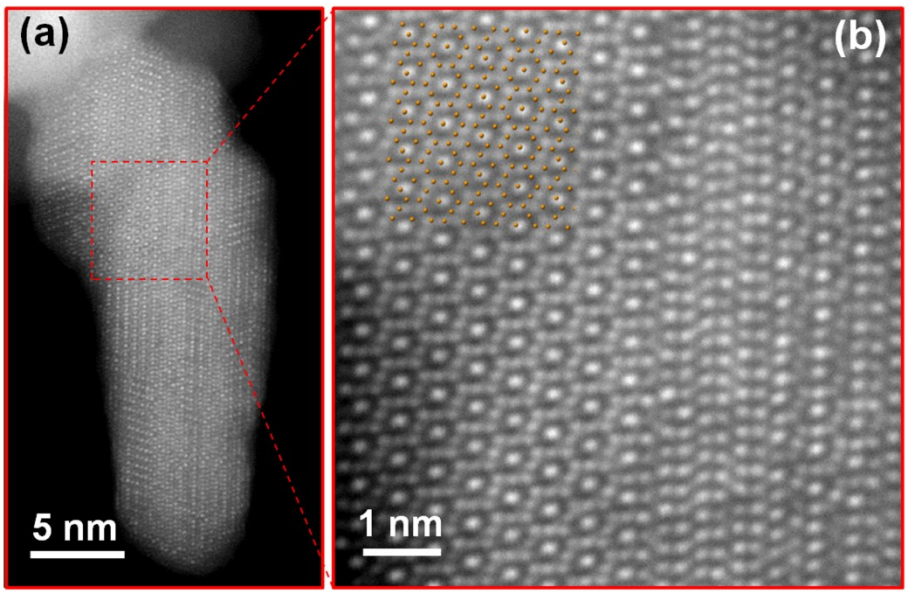

Fig. SI8. HAADF STEM images of SF110 NPL after annealing for 2 hours at 500 °C. The projected model of the spinel ferrite maghemite structure (in <110> zone axis) is superimposed over the image to illustrate the positions of the Fe^{3+} columns.

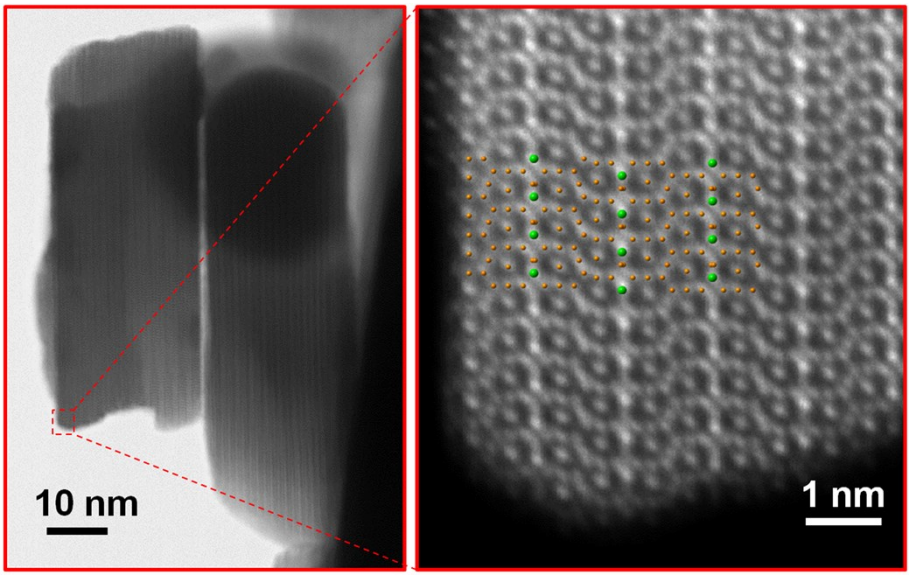

Fig. SI9. BF and HAADF STEM images of NPLs from annealed SF700 sample. The projected model of the magnetoplumbite structure (in <10-10> zone axis) is superimposed over the image to illustrate the positions of the Sr^{2+} and Fe^{3+} columns.

XRD analysis of SF160

The XRD pattern of the SF160 sample was fitted with Topas version 2.1 Bruker AXS 1999. Different trigonal and hexagonal space groups (SGs) were used with the basic repeating unit, determined with the ARM-STEM, as a starting basic unit cell: a = 5.66 Å and c = 9.0 Å. The crystallite sizes were fitted starting from 200 nm. Some of the primitive trigonal SGs, like P-31cs and P-3m, resulted in very good fits (see an example in Fig. SI9a) as well as, for example, the hexagonal SG $P6_3/mmc$ (Fig. SI9b). In all cases the cell parameters were in accordance with those determined with the ARM-STEM, taking account of the expected uncertainty.

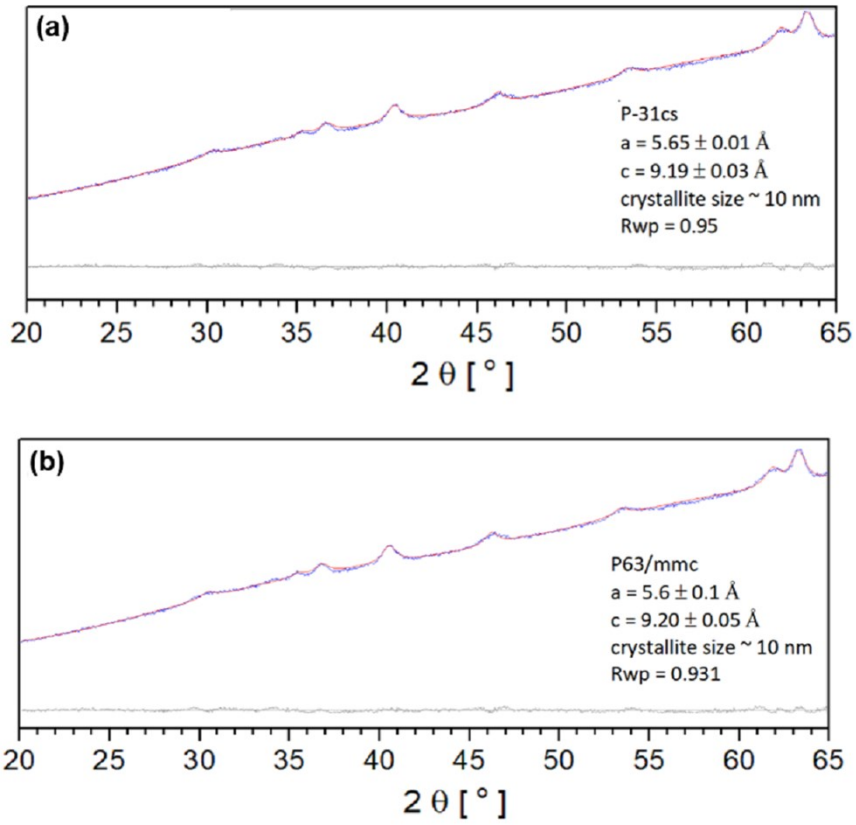

Fig. SI10: Fitted XRD patterns of the SF160 sample with SG P-31cs (163) (a) and with SG $P6_3/mmc$ (194) (b). Blue curves are the measurement; the red curves are fitted; and the grey curves are the difference between the measurement and the fit. Rwp denotes the quality of the fit.

Synthesis of the nanoplatelets at 80 °C

The Sr-ferrite NPLs with new polymorph structure were also synthesized using heating of the suspension of precipitated Sr^{2+} and Fe^{3+} ions for 12 hours at 80 °C. Apart from the synthesis time and the temperature the procedure was equal to that used for the hydrothermal synthesis, which is performed at the temperatures above the boiling point of the reaction medium and at an increased (usually endogenous) pressure.

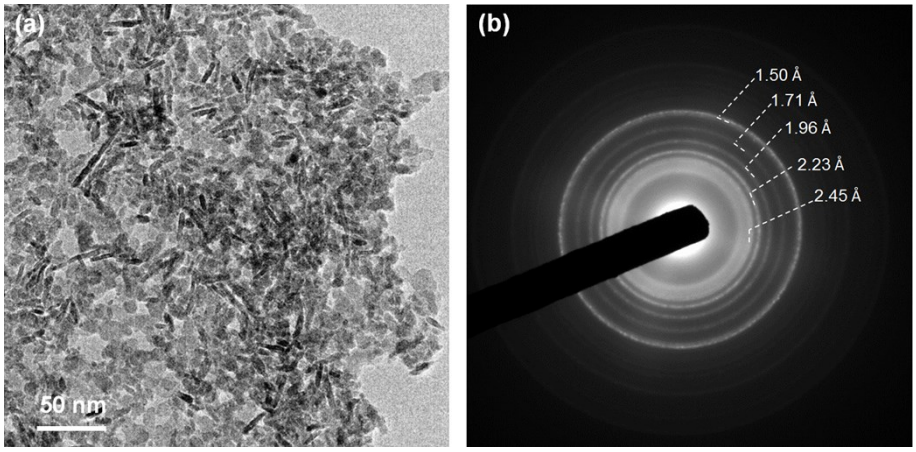

Fig. SI11. TEM image (a) with corresponding electron diffraction pattern (b) of the discoid NPL synthesized by heating the reaction mixture for 12 hours at 80 °C.

References

S1. Lisjak, D.; Hribar Bostjančič, P.; Mertelj, A.; Mavric, A.; Valant, M.; Kovač, J.; Hudelja, H.; Kocjan, A.; Makovec, D.; Formation of Fe(III)-Phosphonate Coatings on Barium Hexaferrite Nanoplatelets for Porous Nanomagnets. ACS Omega 2020, DOI: 10.1021/acsomega.0c01597.

S2. Cornell, R. M.; Schwertmann, U. The Iron Oxides: Structure, Properties, Reactions, Occurrences and Uses; Wiley-VCH: Weinheim, Germany, 2003.

S3. J Kriesel, J.; Lucazeau, G.; Vincent H. Raman Spectra and Vibrational Analysis of BaFe12O19 Hexagonal Ferrite. J. Solid State Chem. 1998, 137, 127—137.

S4. Mazzetti, L.; Thistlethwaite P. J. Raman Spectra and Thermal Transformations of Ferrihydrite and Schwertmannit. J. Raman Spectrosc. 2002, 33, 104–111.

S5. Belec, B.; Dražić, G.; Gyergyek, S.; Podmiljšak, B.; Goršak, T.; Komelj, M.; Nogués, J.; Makovec, D. Novel Ba-Hexaferrite Structural Variations Stabilized on the Nanoscale as Building Blocks for Epitaxial Bi-Magnetic Hard/Soft Sandwiched Maghemite/Hexaferrite/Maghemite Nanoplatelets with Out-Of-Plane Easy Axis and Enhanced Magnetization. Nanoscale 2017, 9, 17551–17560.